

High-fidelity adiabatic quantum computation via dynamical decoupling

Gregory Quiroz

Department of Physics and Center for Quantum Information Science & Technology, University of Southern California, Los Angeles, California 90089, USA

Daniel A. Lidar

Departments of Electrical Engineering, Chemistry, and Physics, and Center for Quantum Information Science & Technology, University of Southern California, Los Angeles, California 90089, USA

(Received 11 May 2012; published 24 October 2012)

We introduce high-order dynamical decoupling strategies for open-system adiabatic quantum computation. Our numerical results for the random-unitary map model demonstrate that a judicious choice of high-order dynamical decoupling method, in conjunction with an encoding which allows computation to proceed alongside decoupling, can dramatically enhance the fidelity of adiabatic quantum computation in spite of decoherence.

DOI: [10.1103/PhysRevA.86.042333](https://doi.org/10.1103/PhysRevA.86.042333)

PACS number(s): 03.67.Lx, 03.65.Yz, 03.67.Pp

I. INTRODUCTION

In adiabatic quantum computation (AQC), a problem is solved by evolving in the ground-state manifold of an adiabatic Hamiltonian $H_{\text{ad}}(t)$, with $t \in [0, T]$ [1,2]. The ground state of the beginning Hamiltonian $H_B = H_{\text{ad}}(0)$ is assumed to be easily preparable, while the ground state of the problem Hamiltonian $H_P = H_{\text{ad}}(T)$ represents the solution to the computational problem. AQC has been shown to be computationally equivalent to the standard circuit model of quantum computation (QC) [3–7] and is being pursued experimentally using superconducting flux qubits [8] and nuclear magnetic resonance [9,10]. However, in spite of evidence of intrinsic robustness [11–16] and proposals to protect AQC against decoherence [17,18], AQC still lacks a complete theory of fault-tolerance, unlike the circuit model of QC [19–24]. In fact, even identifying an acceptable notion of fault-tolerant AQC (FTAQC) is an open problem [25]. To qualify as AQC, at least the *computation* should remain adiabatic. On the other hand, it seems too restrictive to require the techniques used to address decoherence and noise to be adiabatic as well. We thus propose the following characterization of FTAQC: “Given a closed-system AQC specified by H_B and H_P , and $\epsilon > 0$, a fault tolerant open-system simulation will use adiabatic evolution between two faulty encoded Hamiltonians \tilde{H}_B and \tilde{H}_P derived from H_B and H_P , so that the final system-only state of the simulation is efficiently decodable to a state that is ϵ close (in fidelity) to the ground state of H_P . In addition, the simulation may involve any other faulty nonadiabatic error-correction, suppression, or avoidance operations.”

Our characterization is meant to convey that the computation should be adiabatic, and apart from that the error correction can be anything. We make no attempt to rigorously quantify the relation between the “ideal” and “faulty” pairs H_B, H_P and \tilde{H}_B, \tilde{H}_P , the types of allowed error-correction operations, or the nature of the decoding step. Instead, we demonstrate here that it is possible to approach ideal AQC in an open system, using ideas guided by our characterization of FTAQC. Specifically, we shall assume that the underlying *computation* is indeed adiabatic but encoded into new Hamiltonians, and that the *protection* is nonadiabatic.

Reference [18] introduced an AQC protection method which fits this FTAQC approach. Protection is carried out

by means of dynamical decoupling (DD) [26–28] (i.e., the application of strong and frequent pulses to the system), designed to decouple it from the bath. To ensure the compatibility of DD with AQC, all qubits are encoded into a quantum error-detecting code [29], which allows DD pulses to be applied that commute with the adiabatic evolution, while at the same time acting to decouple the system from the bath [30]. Reference [18] relied on first-order DD sequences, resulting in a tradeoff between fidelity and DD sequence bandwidth, and conjectured that high-order DD, in particular concatenated DD (CDD) [31], should alleviate this tradeoff.

Here we demonstrate by using numerical simulations for the random-unitary map model [32] that, following the strategy of Ref. [18] but using high-order DD sequences, and in particular CDD, it is possible to dramatically enhance the fidelity of AQC in an open-system setting. Our results support the idea that FTAQC, in the sense characterized above, is indeed attainable using appropriately chosen DD sequences.

II. ALGORITHMS

We consider two well-known AQC algorithms, which correspond to first- and second-order quantum phase transitions, respectively, and thus to different challenges for AQC [15,33,34]. The first is Grover’s algorithm for the identification of a marked element in an unsorted list of N elements, using the minimum number of oracle queries [35]. This can be done in $O(\sqrt{N})$ queries, which is a quadratic improvement over the best possible classical algorithm [36]. The adiabatic Grover’s algorithm [37,38] is defined by the n -qubit Hamiltonian

$$H_{\text{ad}}^G(t) = [1 - f(t)](I - |u\rangle\langle u|) + f(t)(I - |m\rangle\langle m|), \quad (1)$$

where $|u\rangle$ denotes the uniform superposition over all $N = 2^n$ computational basis states, $|m\rangle$ is the marked state, and I is the identity operator. The minimum spectral gap $\Delta_{\text{min}}^G = O(1/\sqrt{N})$, and the total run time required to reach the ground state $|\Phi_0^G(T)\rangle = |m\rangle$ of $H_{\text{ad}}^G(T)$ is $T \sim O(\sqrt{N})$, provided the optimized interpolation function $f(t) = \frac{1}{2} - \frac{1}{2\sqrt{N-1}} \tan[(1 - 2t/T) \arccos(1/\sqrt{N})]$ is used [37,38].

The second algorithm is 2-SAT on a ring [1,39], represented by the transverse-field Ising model with periodic boundary

conditions:

$$H_{\text{ad}}^{2\text{SAT}}(t) = \left(1 - \frac{t}{T}\right) \sum_{j=1}^n (I - \sigma_j^x) + \frac{t}{T} \sum_{j=1}^n \frac{1}{2} (I - \sigma_j^z \sigma_{j+1}^z), \quad (2)$$

where $\sigma_{n+1}^z \equiv \sigma_1^z$ (σ_j is a Pauli matrix acting on qubit j). The symmetric ground state of $H_{\text{ad}}^{2\text{SAT}}(T)$ is $|\Phi_0^{2\text{SAT}}(T)\rangle = (|0 \cdots 0\rangle + |1 \cdots 1\rangle)/\sqrt{2}$. The minimum gap $\Delta_{\min} = O(1/n)$ occurs near $t = 2T/3$; it can be found using the standard fermionization method [1,40,41].

III. ERROR MODEL

To keep our numerical simulations manageable, we considered a random-unitary map model, which we generated as follows: The ‘‘faulty Hamiltonian’’ is

$$H_0(t) = H_{\text{ad}}(t) + H_{\text{err}}(t), \quad (3)$$

where the error Hamiltonian comprises interactions between the qubits and time-dependent stochastic classical fields:

$$H_{\text{err}}(t) = \sum_{\mu \in \{x,y,z\}} \sum_{j=1}^n \epsilon_j^\mu(t) \sigma_j^\mu. \quad (4)$$

Each field $\epsilon_j^\mu(t)$ is a stationary zero-mean random Gaussian process with spectral density $S_{jk}^{\mu\nu}(\omega) = \delta_{jk} \delta_{\mu\nu} S(\omega)$ [42], where

$$\begin{aligned} S(\omega) &= \frac{1}{\sqrt{2\pi}} \int_{-\infty}^{\infty} \langle \epsilon_j^\mu(t) \epsilon_j^\mu(t + \tau) \rangle e^{i\omega\tau} d\tau \\ &= \sqrt{\frac{J}{2\pi\beta}} \exp[-(\omega/\beta)^2/2], \end{aligned}$$

where $\langle \cdot \rangle$ denotes a Gaussian ensemble average and $S(\omega)$ is t independent due to stationarity. The standard deviation β plays the role of the spectral cutoff ($1/\beta$ is the bath correlation time). The correlation function amplitude satisfies $\langle \epsilon_j^\mu(t) \epsilon_j^\mu(t + \tau) \rangle \propto J\beta$, and in our simulations we chose J so that $\sqrt{\beta J} = \Delta_{\min}/30$ [43].

Each random realization of $H_{\text{err}}(t)$ generates a random unitary $U_\epsilon(t)$, where $\epsilon := \{\epsilon_j^\mu\}$ [the solution of the Schrödinger equation governed by $H_0(t)$] with probability p_ϵ . Applying these unitaries to a fixed initial state ρ_0 is equivalent to the completely positive random-unitary map $\sum_\epsilon A_\epsilon \rho_0 A_\epsilon^\dagger$ with Kraus operators $A_\epsilon := \sqrt{p_\epsilon} U_\epsilon$ [44]. While this is not the most general model of decoherence [32], it represents an interesting and relevant error model (e.g., due to charge noise in superconducting qubits [45–47]).

IV. DYNAMICAL DECOUPLING

The problem we attempt to solve using DD is to perform high-fidelity AQC in spite of the presence of H_{err} . The decoupling pulses are introduced through an additional time-dependent control Hamiltonian $H_C(t)$, which generates a unitary pulse propagator $U_C(t)$. We consider zero-width pulses separated by finite intervals [48]. The inclusion of pulse-width errors is left for a future study focusing on a more complete picture of fault tolerance; CDD is known to be relatively

robust against such errors [31,49,50]. The Hamiltonian $H(t) = H_C(t) + H_0(t)$ generates the complete dynamics of the system in the presence of DD, represented by the unitary evolution operator $U(t,0)$. To suppress $H_{\text{err}}(t)$ while preserving $H_{\text{ad}}(t)$, we require that each term in $H_{\text{err}}(t)$ anticommute with some pulse operator comprising $H_C(t)$, while $[H_C(t), H_{\text{ad}}(t')] = 0 \forall t, t'$. Upon satisfying these conditions the time evolution operator in the $H_C(t)$ -interaction picture becomes

$$\begin{aligned} \tilde{U}(T) &:= U_C^\dagger(T) U(T) \\ &= \mathcal{T} e^{-iT \int_0^1 H_{\text{ad}}(s) ds} + O[(\|\tilde{H}'_{\text{err}}\| T)^{\alpha+1}], \end{aligned} \quad (5)$$

where \mathcal{T} denotes time ordering and \tilde{H}'_{err} is an effective error Hamiltonian, which can be computed using the Magnus series [51]. DD becomes effective provided the ‘‘noise strength’’ $\|\tilde{H}'_{\text{err}}\| T < 1$ [49]. The larger the ‘‘decoupling order’’ α , the closer to ideal is the adiabatic evolution. Previously only the case $\alpha = 1$ was analyzed [18].

A. Stabilizer decoupling

To satisfy the noninterference condition $[H_C(t), H_{\text{ad}}(t')] = 0$ we make use of the $[[n, n-2, 2]]$ stabilizer code \mathcal{C} , encoding $n-2$ logical qubits (n even) into n physical qubits [18,29,52]. The stabilizer of \mathcal{C} is $\mathcal{S} = \{I, X, Y, Z\}$, where $X(Y, Z) = \bigotimes_{j=1}^n \sigma_j^{x(y,z)}$. The encoded single-qubit operators are $\bar{\sigma}_j^x = \sigma_1^x \sigma_{j+1}^x$ and $\bar{\sigma}_j^z = \sigma_{j+1}^z \sigma_n^z$, where $j = 1, 2, \dots, n-2$. AQC over \mathcal{C} is implemented by replacing each Pauli matrix in $H_{\text{ad}}(t)$ by its encoded version, yielding an encoded adiabatic Hamiltonian $\bar{H}_{\text{ad}}(t)$ which is fully 2 local.

B. Concatenated dynamical decoupling for adiabatic quantum computation

Consider a unitary decoupling group $\mathcal{G} = \{g_k\}_{k=1}^G$ chosen to implement first-order decoupling ($\alpha = 1$). DD effectively averages out H_{err} by symmetrizing it over \mathcal{G} [27,28]. We choose $\mathcal{G} = \mathcal{S}$ and hence $G = 4$ for the $[[n, n-2, 2]]$ code. CDD achieves higher-order decoupling by concatenating this symmetrization, so that each additional level averages out the remaining leading order. So far, CDD has been defined only for piecewise constant Hamiltonians [31,49,53]. Adapting CDD to incorporate the time-dependence of $H(t)$, we have at the $l+1$ st level of concatenation

$$U_{\text{CDD}}^{(l+1)}(T) = \prod_{k_1=1}^G g_{k_1} P_{k_1}^{(l)} g_{k_1}^\dagger, \quad l \geq 0. \quad (6)$$

Starting from $m = 2$, $P_{k_1}^{(l)}$ is calculated recursively from

$$P_{k_1, \dots, k_{m-1}}^{(l)} := \prod_{k_m=1}^G g_{k_m} P_{k_1, \dots, k_m}^{(l-1)} g_{k_m}^\dagger, \quad l \geq 1 \quad (7)$$

with DD-free evolution segments

$$\begin{aligned} P_{k_1, \dots, k_l}^{(0)} &:= U_0 \left(t_{l-1} + T \frac{k_l}{G^l}, t_{l-1} + T \frac{k_l - 1}{G^l} \right), \\ t_l &:= T \sum_{j=1}^l \frac{k_j}{G^j}, \quad t_0 = 0, \quad l \geq 1, \end{aligned} \quad (8)$$

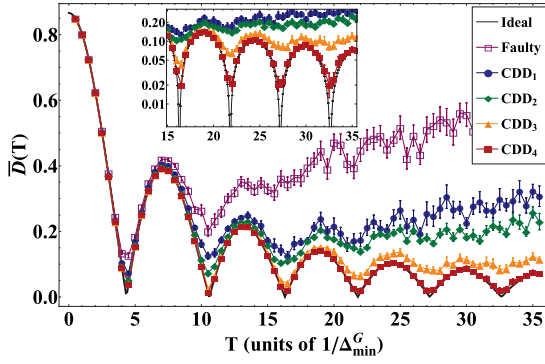


FIG. 1. (Color online) Averaged trace-norm distance $\overline{D}(T)$ between the CDD-protected final state and the desired ground state as a function of total run time T for Grover's algorithm, in units of the inverse minimum gap. Cutoff frequency is $\beta = \Delta_{\min}/5$. The ideal (solid black) and faulty (empty squares) evolutions are included for reference. Inset shows a closeup for large T , using a log scale for the vertical axis. Performance improves monotonically with concatenation level l , with the corresponding sequence denoted CDD_l . Error bars are due to averaging over 30 random realizations of $H_{\text{err}}(t)$.

where the DD-free evolution operator is $U_0(t_a, t_b) = T \exp[-i \int_{t_b}^{t_a} dt H_0(t)]$. These definitions ensure that at concatenation level l the symmetrization procedure is applied to DD-free evolution segments of duration $\tau_l = T/G^l$, using a total of G^l pulses. For piecewise-constant Hamiltonians it has been shown that CDD achieves $\alpha = l$ th order decoupling [49,50,53–55].

C. QDD for adiabatic quantum computation

Another way to achieve high-order decoupling in a multi-qubit setting is quadratic DD (QDD) [56], which is obtained by nesting two Uhrig DD [57] (UDD) sequences

$$U_{\text{QDD}}^{(M_1, M_2)}(T) = U_{\text{UDD}, \Omega_2}^{(M_2)} \circ U_{\text{UDD}, \Omega_1}^{(M_1)} \circ U_0(T), \quad (9)$$

where $U_{\text{UDD}, \Omega}^{(M)} \circ U_0(T) = \Omega^{M+1} \prod_{k=1}^{M+1} \Omega U_0(\delta_k^{(M)}, \delta_{k-1}^{(M)})$, and where $\delta_k^{(M)} = T \sin^2[k\pi/(2M+2)]$ and $\Omega_1 \neq \Omega_2 \in \{X, Z\}$ are the generators of \mathcal{S} . The number of pulses in each sequence, or sequence order, is $\{M_1, M_2\}$ and dictates the decoupling order α , requiring only $(M_1+1)(M_2+1)$ total pulses for $\alpha \geq \min(M_1, M_2)$ [58–60].

V. RESULTS

For each algorithm (Grover, 2-SAT) we used $n = 4$ physical qubits to encode two logical qubits in the code \mathcal{C} and studied both CDD- and QDD-protected AQC. In our simulations the pulse intervals decrease as the total number of pulses increases with the concatenation or QDD sequence order, for each given value of the total time T . Starting for both algorithms from the uniform superposition state as the initial encoded state $|\psi(0)\rangle$, we computed $|\psi_\epsilon(T)\rangle = U_{\text{xDD}, \epsilon}(T) |\psi(0)\rangle$, where $x = C$ or Q [Eqs. (6) and (9)] for a given Gaussian noise realization ϵ . We assessed performance using the trace-norm distance $D_\epsilon(T) := D[|\psi_\epsilon(T)\rangle, |\Phi_0(T)\rangle] = [1 - F_\epsilon^2(T)]^{1/2}$ [61], where $F_\epsilon(T) = |\langle \psi_\epsilon(T) | \Phi_0(T) \rangle|$ is the fidelity, to quantify

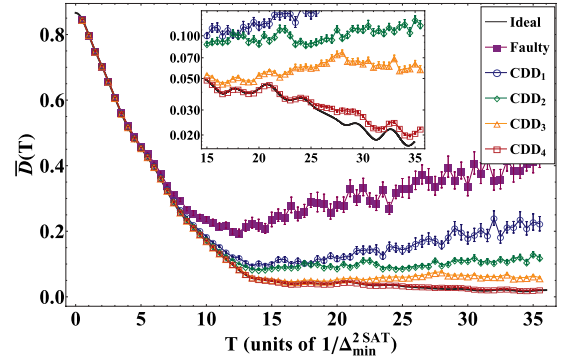


FIG. 2. (Color online) As in Fig. 1, for the 2-SAT on a ring problem. The curves for ideal evolution and CDD_4 overlap to within our numerical accuracy up to $T = 25/\Delta_{\min}^{2\text{SAT}}$. Note the minimum at $T \approx 12\Delta_{\min}^{2\text{SAT}}$ for the faulty evolution, suggesting the existence of an optimal open-system evolution time. This optimal time increases with concatenation level, until it disappears in the ideal case and for CDD_4 . CDD boosts the deviation by a factor of 10 from $\overline{D} \approx 0.2$ (at $T \approx 12.5/\Delta_{\min}^{2\text{SAT}}$) in the faulty case to $\overline{D} \approx 0.02$ (at $T \approx 34.5/\Delta_{\min}^{2\text{SAT}}$) for CDD_4 .

the difference between the encoded, xDD-protected state $|\psi_\epsilon(T)\rangle$ and the desired encoded final state $|\Phi_0(T)\rangle$ [i.e., the ground state of $\overline{H}_{\text{ad}}(T)$]. All our plots exhibit the average distance $\overline{D}(T) = \sum_\epsilon p_\epsilon D_\epsilon(T)$, and it is easily verified that $1 - \overline{D}(T)$ lower bounds the output fidelity of the random-unitary map with Kraus operators $\sqrt{p_\epsilon} U_{\text{xDD}, \epsilon}(T)$ [44]. In the ideal case of noise- and DD-free evolution, $|\psi_{\text{ad}}(t)\rangle = T \exp[-i \int_0^t \overline{H}_{\text{ad}}(t') dt'] |\psi_{\text{ad}}(0)\rangle$ [where $|\psi_{\text{ad}}(0)\rangle = |\Phi_0(0)\rangle$], the adiabatic theorem [62] guarantees $D[|\psi_{\text{ad}}(T)\rangle, |\Phi_0(T)\rangle] \ll 1$ provided $T \gg \max_{s \in (0,1)} \|\frac{d}{ds} \overline{H}_{\text{ad}}\|^{b-1} / \Delta_{\min}^b$, $s = t/T$, $b \in \{1, 2, 3\}$ [63–65] (see Appendix A). In our simulations a finite range of T s was used; as can be seen from Figs. 1–3, $\overline{D}(T)$ does indeed tend to zero for the ideal case as T increases, although not monotonically in the Grover case [66]. The main effect of $H_{\text{err}}(t)$ is to cause $\overline{D}(T)$ to diverge away from zero as T increases, so that there is an optimal evolution time [67]. The main role of DD protection, then, is to keep the fidelity of the AQC process as close as possible to the ideal and, in particular, to prevent $\min_{T \in [0, T_{\text{max}}]} \overline{D}(T)$ from growing larger than some tolerance $\epsilon > 0$ away from $\min_{T \in [0, T_{\text{max}}]} D[|\psi_{\text{ad}}(T)\rangle, |\Phi_0(T)\rangle]$. This is the sense in which DD-protected AQC approaches the ideal of FTAQC described in the introduction.

CDD results for Grover's problem are shown in Fig. 1 for increasing concatenation levels, at $\beta = \Delta_{\min}/5$. The faulty Grover evolution [generated by $\overline{H}_{\text{ad}}^G(t) + H_{\text{err}}(t)$] reaches a minimum deviation $\overline{D}(T) \approx 0.13$ at $T \approx 4.5/\Delta_{\min}^G$ and then diverges from the ideal evolution [generated by $\overline{H}_{\text{ad}}^G(t)$]. In contrast, CDD-protected evolution becomes remarkably close to the ideal evolution as the level of concatenation increases. Nearly ideal evolution is maintained essentially over the entire range of T values we simulated.

Figure 2 shows our CDD results for the 2-SAT problem. CDD-protected evolution is essentially indistinguishable from the ideal at sufficiently high concatenation level. The improved

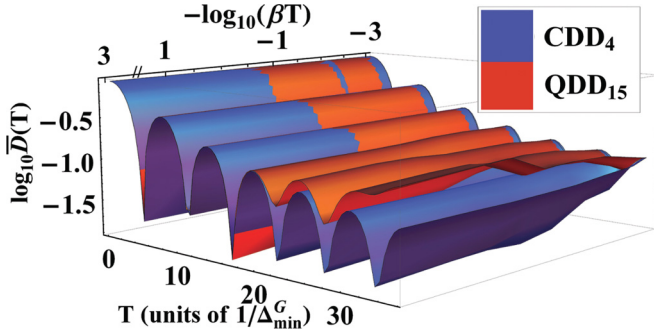


FIG. 3. (Color online) CDD_4 vs QDD_{15} for the Grover problem as a function of the normalized bath correlation time $1/(\beta T)$ and normalized total run time T/Δ_{\min}^G . Increasing the bath correlation time $1/\beta$ at fixed T generally results in improved performance for CDD_4 , whose performance is significantly better than QDD_{15} in the large- T regime. All results were averaged over 30 realizations of $H_{\text{err}}(t)$.

performance in the 2-SAT case, relative to the Grover case, is consistent with earlier observations that algorithms associated with second-order quantum phase transitions are more amenable to AQC than those for first-order transitions [15,33,34].

Along with CDD, we analyzed QDD-protected AQC for $M_1 = M_2 = M \in \{1, 3, 6, 7, 14, 15\}$, where the odd sequence orders correspond to the first four levels of concatenation in CDD_l , $l \in \{1, 2, 3, 4\}$, respectively, having the same number of pulses $[(M+1)^2$ and $4^l]$. CDD and QDD are compared in our simulations at equal T values. QDD $_M$ performance improves monotonically for sufficiently large β (not shown), but we find that QDD_{15} performance is consistently inferior to that of CDD_4 in the adiabatic regime of large $T \Delta_{\min}$, as can be seen in Fig. 3. This is surprising in light of the aforementioned fact that in their non-AQC roles as quantum memory DD sequences, the respective decoupling orders of CDD_l and QDD_M are l and $\geq M$. We have confirmed that the results for the 2-SAT problem are qualitatively similar, again favoring CDD (see Appendix B for further details).

In Figs. 1 and 2 the cutoff frequency β was fixed. Performance dependence on β is shown in Fig. 3 and is seen to be mild for CDD_4 at each fixed value of T . The dependence on β is further elucidated in Fig. 4, which shows that performance generally improves as β shrinks, as expected. In contrast, QDD_{15} results show almost no dependence on β , and the $\min_{\tau} \bar{D}(T(\tau))$ values are approximately twice as large as those obtained for CDD_4 (see Appendix C for further details). In essence, the superior performance of CDD can be explained by recognizing that QDD is designed to suppress the system-bath coupling at the end of the pulse sequence, while CDD performs this suppression recursively all throughout the evolution. This is a better fit for AQC, with its time-dependent system Hamiltonian (see Appendix D for further details).

VI. CONCLUSION AND FUTURE WORK

We have introduced a high-order DD-based strategy for protected open-system AQC and demonstrated using numerical simulations that it is capable of achieving high fidelities for a

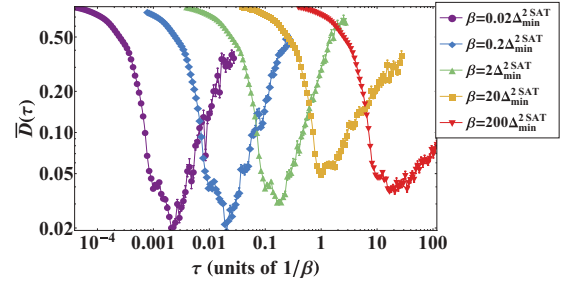


FIG. 4. (Color online) Performance of CDD_4 -protected evolution for the 2-SAT problem, as a function of pulse interval τ , for different values of the frequency cutoff β (τ in units of $1/\beta$ to separate the curves). Total time $T = 4^4 \tau$. The minimum in each fixed β curve corresponds to an optimal pulse interval $\tau_{\text{opt}}(\beta)$, and corresponding $T_{\text{opt}}(\beta)$. Peak performance $\bar{D}(T_{\text{opt}}(\beta))$ improves as β is decreased, except at $\beta = \Delta_{\min}^{2\text{SAT}}/0.005$ where self-averaging effects result from rapid fluctuations in $\epsilon_j^{\mu}(t)$ (“motional narrowing”). Results are averaged over 30 realizations of $H_{\text{err}}(t)$.

random-unitary map model. At sufficiently high concatenation level, the CDD-based protection strategy achieves fidelities which are essentially indistinguishable from closed-system adiabatic evolution for two algorithms associated with first- and second-order quantum phase transitions. CDD outperforms QDD in our simulations; an effect which can be attributed to CDD’s ability to remove errors throughout the evolution, as opposed to just at its end. Future work should elucidate the question of scaling of CDD resources with problem size, consider finite-width DD pulses, and generalize the results to more general decoherence models.

ACKNOWLEDGMENTS

We are grateful to Dr. G. Paz-Silva for important discussions. This research was supported by the Department of Defense, the Lockheed Martin Corporation under the URI program, and by NSF Grants No. CCF-0726439, No. CHE-924318, No. CHM-1037992, No. PHY-969969, and No. PHY-803304. The views and conclusions contained in this document are those of the authors and should not be interpreted as representing the official policies, either expressly or implied, of the US Government.

APPENDIX A: ADIABATIC THEOREM

Let $s := t/T$ denote the dimensionless time, pick $q \in (0, 1)$, and assume that the total adiabatic evolution time satisfies

$$T \gtrsim \frac{a (\max_s \|dH/ds\|)^{b-1}}{q \Delta_{\min}^b}. \quad (\text{A1})$$

Then, according to the adiabatic theorem,

$$D[|\psi(T)\rangle, |\Phi_0(T)\rangle] \lesssim q^a. \quad (\text{A2})$$

The values of the integer exponents a and b in Eqs. (A1) and (A2) depend upon the differentiability and analyticity properties of $H(t)$ and the boundary conditions satisfied by its derivatives [63–65]; typically $b \in \{1, 2, 3\}$ [63], while a can be tuned between 1 and arbitrarily large integer values, equal to

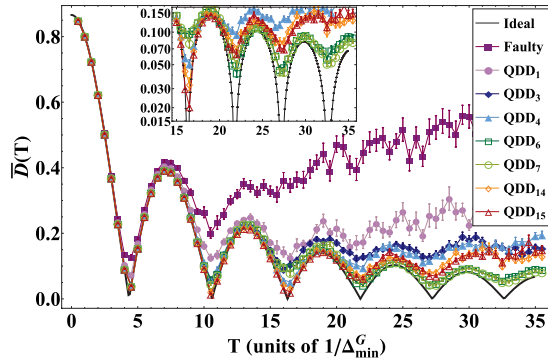


FIG. 5. (Color online) Trace-norm distance between the QDD-protected final state $\rho(T)$ and the desired ground state ρ_M as a function of total run time T for Grover's algorithm, in units of the inverse minimum gap. Specific sequence orders are considered: $M = 1, 3, 4, 6, 7, 14, 15$. Odd-parity sequence orders contain a number of pulses equal to those of the CDD sequences shown in Fig. 1 (main text). In contrast to CDD, QDD-protected evolution does not more closely resemble closed-system evolution at large T as the number of pulses grows.

the number of vanishing derivatives of $H(t)$ at the boundaries $t = 0$ and $t = T$ [64].

APPENDIX B: QDD PERFORMANCE

In Sec. V we briefly discussed the performance for QDD-protected AQC for both algorithms: Grover's search problem and 2-SAT on a ring. Here, we elaborate on those results and present some of our numerical results. We consider the case of equal inner and outer sequence orders, $M_j = M$, $j = 1, 2$, to efficiently combat the uniform decoherence model of Eq. (2). The sequence orders are chosen as $M = 1, 3, 6, 7, 14, 15$, where the odd-parity orders correspond to the first four levels of concatenation in CDD, $l = 1, 2, 3, 4$, respectively. The two contrasting DD schemes are compared with respect to pulse arrangement (concatenation versus nesting) and interpulse delay, while total time and the number of pulses are equivalent.

In Fig. 5, the results for QDD-protected Grover are shown for $\beta = \Delta_{\min}/5$. Closed-system-like behavior is observed for $M = 1, 3, 6, 7$ and $M = 14, 15$ up to $T \approx 4.5/\Delta_{\min}^G$ and $T \approx 11.5/\Delta_{\min}^G$, respectively, where the minimum deviation $\min_T \bar{D}(T)$ generally decreases with increasing sequence order. QDD does not achieve a higher performance than CDD for an equivalent number of pulses, as CDD minimum deviations range from 10% to 15% smaller than QDD values at equivalent "optimal" values of T . QDD is also distinct from CDD in its behavior at large T , with respect to the simulated range, where QDD-protected evolution begins to diverge from the ideal closed-system evolution as the number of pulses increases. Although the performance of each scheme, designated by the minimum deviation, is well characterized in the small- T regime for Grover, this characteristic of QDD could ultimately lead to a bound on QDD effectiveness for algorithms where DD extends ideal-like behavior to larger values of T .

Interestingly, 2-SAT on a ring is one such case where the large- T regime is relevant and QDD performance diminishes

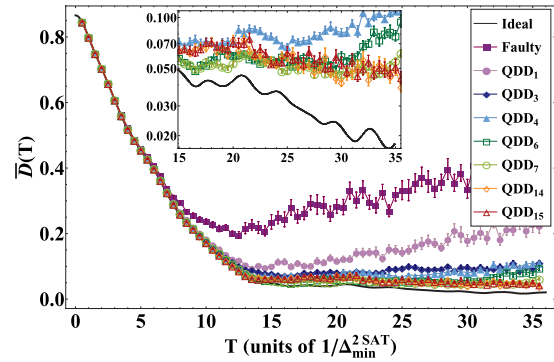


FIG. 6. (Color online) Same as in Fig. 5, for the 2-SAT on a ring problem. QDD protection extends ideal evolution as sequence order increases, ultimately saturating at $M = 14$.

at a critical value of sequence order. As with Grover, a general trend of decreasing $\min_T \bar{D}(T)$, with increasing sequence order exists for all $M \leq 14$ considered here. However, the appealing relationship between minimum deviation and M disappears for 2-SAT at $M = 15$, where the minimum deviation is nearly 15% larger than that of $M = 14$. [See Fig. 6 for numerical results.] The values of T associated with the minimum deviation, $\arg \min_T \bar{D}(T)$, extend far into the large- T regime and reach a maximum of $T \approx 35.5/\Delta_{\min}^{2SAT}$ for $M = 14, 15$. In the case of CDD at $\ell = 4$, the maximum T value is nearly equivalent ($[T \approx 34.5/\Delta_{\min}^{2SAT}]$), yet CDD-protected evolution does not exhibit a divergence within the simulated range and obtains a minimum deviation of approximately half that of $M = 14, 15$. The bound on QDD performance is indicative of a preference to concatenation rather than nesting, perhaps most notably for algorithms with second-order quantum phase transitions, due to the recursive suppression of the system-bath interaction throughout the entire evolution provided by the former.

APPENDIX C: DEPENDENCE OF DD PERFORMANCE ON CUTOFF FREQUENCY

One contributor to the better performance of CDD is the Gaussian spectral density of the noise process $\epsilon_j^\mu(s)$; the performance of UDD-based schemes is adversely affected if the spectral cutoff is not sufficiently sharp at high frequencies [68,69]. Transforming the error Hamiltonian into the toggling frame and analyzing the resultant DD modulation functions in the frequency domain, one finds that DD can be interpreted as a high-pass filter whose cutoff frequency increases as the interpulse free evolution period decreases [70]. UDD-based schemes tend to have the flattest filter functions [46,69], and hence their cutoff frequencies are much smaller than concatenation-based schemes. Here, we examine the effects of the spectral cutoff β on QDD and CDD-protected AQC for both Grover's search problem and 2-SAT on a ring.

First, let us consider the performance of CDD and QDD as a function of the total adiabatic run time T and normalized correlation time $(\beta T)^{-1}$. We focus on the sequences which exhibit the smallest minimum deviation between DD-protected and ideal evolution for both schemes: CDD₄ and QDD₁₅

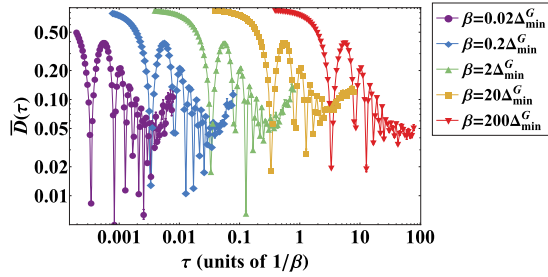


FIG. 7. (Color online) Performance of CDD_4 for Grover's search algorithm as a function of the pulse interval τ for various values of the frequency cutoff β . Short correlation times ($\beta = 200\Delta_{\min}^G$) demand a large pulse interval to obtain minimum deviation from ideal evolution. As β is decreased, reduced minimum deviation is achieved at pulse intervals much smaller than the correlation time ($1/\beta$). Results are averaged over 30 realizations of H_{err} .

for Grover and CDD_4 and QDD_{14} for 2-SAT. In Figs. 3 (main text) and 10, the deviation of DD-protected evolution from ideal AQC evolution is shown for both sequences in the case of Grover's search algorithm and for 2-SAT on a ring, respectively. The normalized correlation time $(\beta T)^{-1} \in [10^{-3}, 10^3]$ and the total run time is varied from $T = 0$ to $T = 36/\Delta_{\min}$. We average all results over 30 random realizations of $\epsilon_j^\mu(s)$.

In the case of Grover's search algorithm, CDD_4 dominates for short correlation times while QDD_{15} performance increases substantially at large $(\beta T)^{-1}$ and attains minimum deviations approximately equal to CDD_4 . CDD_4 -protected and closed-system evolution nearly coincide up to T values ranging from $T \approx 4.5/\Delta_{\min}^G$ at $(\beta T)^{-1} = 10^{-3}$ to $T \approx 16.5/\Delta_{\min}^G$ at $(\beta T)^{-1} = 10^3$, where the minimum deviation reduces by about 36% over the entire range of $(\beta T)^{-1}$. QDD_{15} obtains similar values of T ; however, minimum deviation reduces by about 60% over the range of cutoff frequencies. The distinction between the DD schemes is most notable in the large- T regime, where QDD_{15} -protected evolution diverges from the ideal evolution more dramatically than CDD_4 as the spectral cutoff is reduced. However, this effect is inconsequential for QDD_{15} performance since minimum deviation occurs predominantly in the short- T regime. Additional artifacts, such as self-averaging due to rapid fluctuations of $\epsilon_j^\mu(s)$ at short correlation times ("motional narrowing") are also present for both schemes.

The results for the 2-SAT problem differ from Grover's algorithm in that CDD_4 maintains its superiority over QDD_{14} for all β . CDD-protected evolution reaches minimum deviation at $T \approx 28/\Delta_{\min}^{2\text{SAT}}$ and $T \approx 34.5/\Delta_{\min}^{2\text{SAT}}$ for $(\beta T)^{-1} = 10^{-3}$ and $(\beta T)^{-1} = 10^3$, respectively, where the value of $\min_T \bar{D}(T)$ reduces by 56% over the entire range of $(\beta T)^{-1}$ considered. Similar values of T corresponding to $\arg \min_T \bar{D}(T)$ are also obtained for QDD; however, the dramatic reduction in minimum deviation with decreasing β is not observed. In fact, even for the largest normalized correlation time $(\beta T)^{-1} = 10^3$ QDD_{14} minimum deviation remains approximately 50% larger than CDD_4 . As discussed in Sec. B, increasing the sequence orders of QDD does not appear to be beneficial for the 2-SAT problem due to the divergent behavior of QDD-protected

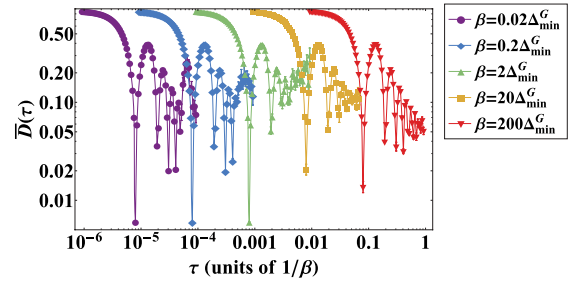


FIG. 8. (Color online) As in Fig. 7, for QDD_{15} . The pulse interval τ represents the *minimum* delay between pulses for QDD. In contrast to CDD_4 , minimum deviation between DD-protected and ideal evolution does not increase with correlation time for QDD. Note also that the minimum deviations are approximately twice as large as those obtained for CDD and require a minimum pulse interval 10 times smaller.

evolution from the ideal case at large T . Here, we show that similar results are found for a wide range of cutoff frequencies. We suspect that similar results would be obtained for any algorithm where DD-protection extends ideal-like behavior to large- T values.

The expectation of spectral cutoff-dependent variations in DD performance is clearly evident for both Grover's algorithm and 2-SAT. The minimum deviations for CDD_4 and QDD_{15} decrease with increasing correlation time for the Grover case, with QDD_{15} obtaining the more significant reductions over the range of β considered. Closed-system-like evolution is observed for extended time durations, dependent upon correlation time, in the case of 2-SAT for both CDD_4 and QDD_{14} , with CDD_4 maintaining the more favorable minimum deviations. The attributes of DD-protected AQC appear to be dependent upon the order of the quantum phase transition; however it is necessary to consider additional algorithms to truly validate this observation. Whether or not such a conclusion can be drawn, the algorithm-dependent variations in DD performance are still quite intriguing, and perhaps unexpected, results.

As an additional analysis, we consider DD performance with respect to the minimum delay between successive pulses τ for various values the spectral cutoff β . The minimum pulse delay is a canonical parameter that represents a physical constraint in standard DD studies, where the primary objective is to apply the control pulses such that $\beta\tau \ll 1$ in order to generate the desired effective averaging of H_{err} to some order in τ (or T) [26,31,49,53,56]. This condition on τ presents a contradictory situation for AQC, where extended total evolution time is demanded to obtain higher computational accuracy. Although previous work has addressed this issue for the case of periodic DD (PDD), a general understanding of the relationship between τ and β for AQC evolution is still lacking for more sophisticated DD schemes. By varying the spectral cutoff, we seek to gain insight into the connection between β and the value of τ where minimum deviation between DD-protected and ideal evolution occurs, $\tau_{\text{opt}} = \arg \min_{\tau} \bar{D}(\tau)$, specifically for CDD and QDD.

First, consider Grover's search problem for CDD_4 and QDD_{14} as a function of τ shown in Figs. 7 and 8, respectively.

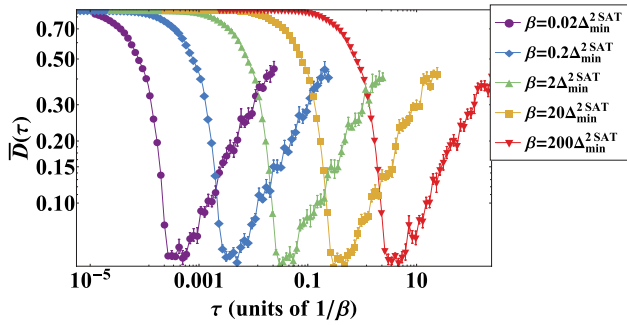


FIG. 9. (Color online) As in Fig. 4 (main text), for QDD₁₄. Here, the pulse interval τ represents the *minimum* delay between pulses. Minimum deviations from ideal evolution are approximately twice as large as those obtained for CDD₄. Peak performance appears insensitive to the value of β .

CDD₄-protected evolution clearly exhibits a direct relationship between the minimum deviation from ideal evolution and β , generally reducing as the spectral cutoff reduces. Large spectral cutoffs ($\beta = 200\Delta_{\min}^G$) require a relatively large pulse delay, $\tau_{\text{opt}} \approx 10/\beta$, to generate an evolution long enough to reach minimum deviation. Consequently, the $\beta\tau \ll 1$ condition is violated and DD-protected evolution deviates more significantly from ideal evolution, $D \approx 0.02$ at the lowest point. Short spectral cutoffs ($\beta = 0.02\Delta_{\min}^G$) result in a τ_{opt} approximately 1000 times smaller than $1/\beta$ and a considerable reduction in the minimum deviation, $D \approx 0.005$. The β dependence of QDD₁₅ is clearly noticeable when transitioning into $\beta\tau \ll 1$, yet the reduction in minimum deviation is unsubstantial thereafter. Peak performance occurs for $\beta = 0.02\Delta_{\min}^G$, where τ_{opt} is about 10^5 times smaller than $1/\beta$. In general, minimum deviation is reached at minimum pulse intervals of approximately 10 times smaller than those obtained for CDD₄.

The results are qualitatively equivalent for the 2-SAT problem, as displayed in Figs. 4 (main text) and 9, for CDD₄ and QDD₁₄, respectively. The minimum deviation and τ_{opt} decrease with decreasing spectral cutoff for CDD₄, while appreciable changes in the minimum D are not observed for QDD₁₄. Again, large spectral cutoffs require minimum pulse intervals that are longer than $1/\beta$ ($\tau_{\text{opt}} \approx 10/\beta$ for $\beta = 200\Delta_{\min}^{2\text{SAT}}$) to acquire the total time necessary to reach minimum deviation. Self-averaging effects are more noticeable for 2-SAT and contribute to the improvement in CDD₄ performance seen in Fig. 4 (main text) for $\beta = 200\Delta_{\min}^{2\text{SAT}}$ since $\beta\tau_{\text{opt}} > 1$. In contrast to the Grover case, the values of τ_{opt} are comparable for both sequences, which is consistent with the extended ideal-like AQC evolution observed for increasing correlation time in Fig. 10. Furthermore, a distinction can be made between Grover and 2-SAT with respect to their susceptibility to variations in β . CDD₄-protected AQC significantly improves with increasing correlation time for 2-SAT, whereas the performance variations are less dramatic for the Grover case.

APPENDIX D: EFFECT OF $H_{\text{ad}}(s)$ -INDUCED NOISE

An additional contributor to the favorable performance of CDD is the scheme's effectiveness in suppressing decoherence

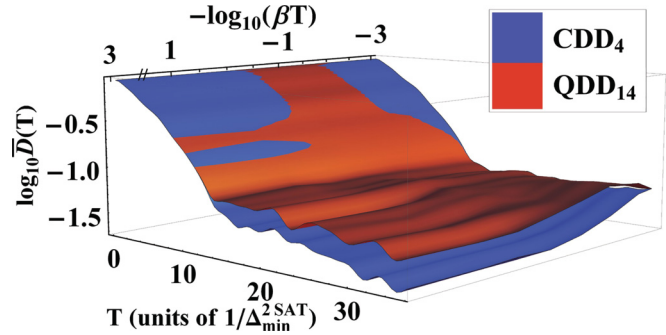


FIG. 10. (Color online) Comparison between CDD₄ and QDD₁₄ performance for 2-SAT on a ring as a function of the normalized correlation time $(\beta T)^{-1}$ and total run time T . As in Fig. 3 (main text), sequence performance is nearly the same for short correlation times. Increases in correlation time result in smaller deviations between DD-protected and ideal evolution for both schemes.

associated indirectly with the time-dependent interpolation function $f(s)$. Although $H_{\text{ad}}(s)$ is, of course, by design not an error-generating term, at second order in the Magnus expansion it couples to H_{err} via a double commutator of the form $[[H_{\text{ad}}(s), H_{\text{err}}], H_C(s)]$. Focusing on the case where the error model is time independent, $\epsilon_j^\mu(s) \equiv \epsilon$, we analyze the interplay between DD and $f(s)$ for Grover's problem, where the interpolation function is nonlinear.

In Figs. 11 and 12, we show the performance of CDD and QDD-protected AQC, respectively, for $\epsilon = 10^{-2}$. The faulty evolution only coincides with the ideal case up to $T \approx 4/\Delta_{\min}^G$, thereafter diverging rapidly. Protecting AQC by CDD does not appear to be beneficial until $\ell = 4$, where CDD₄-protected evolution closely coincides with ideal evolution throughout the simulated range of T . The results for QDD-protected AQC are quite different in that increasing the number of pulses does not necessarily prolong ideal evolution, nor reduce the minimum deviation. Significant deviations from ideal evolution are observed for all $M \neq 15$ when $T \leq 25/\Delta_{\min}^G$, while $M = 6$ appears to be optimal for $T \geq 25/\Delta_{\min}^G$. Interestingly, the evolution generated by $M = 15$ produces the longest closed-system-like evolution and the most considerable divergence from the ideal case.

The fact that the optimal interpolation function for Grover's search is a nonlinear function most likely dictates the bias in DD scheme. The function $f(s)$ essentially plays the role of a time-dependent noise process that increases rapidly throughout the AQC evolution, except near the minimum energy gap. As with the time-dependent $\epsilon_j^\mu(t)$ functions, CDD is better equipped to deal with $f(s)$ -induced decoherence due to the recursive error suppression provided by each sublevel of concatenation. In contrast, UDD protocols do not complete the error averaging process until the last pulse is applied: not all error channels are addressed by each nested sequence. The procedure appears to be most detrimental for increasing sequence orders at relatively large values of T , which implies that the nonlinearity of $f(s)$ is generating effective Hamiltonians at each nested sublevel that cannot be averaged out completely. This result is quite similar to the spectral cutoff analysis shown in Fig. 8 for QDD₁₅, where minimum deviation grew considerably for short correlation

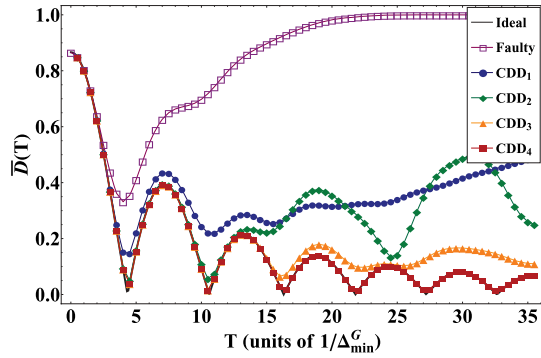


FIG. 11. (Color online) Performance of CDD for a constant error Hamiltonian [$\epsilon_j^\mu(s) \equiv 10^{-2} \forall \mu, j$ in Eq. (2) (main text)]. The curves for ideal evolution, faulty evolution, and CDD₄ overlap up to $T \approx 4/\Delta_{\min}^G$, after which CDD₄ continues to track the ideal evolution essentially perfectly throughout the simulated range.

times, most notably at $\beta = 20\Delta_{\min}^G$, due to rapid fluctuations in $\epsilon_j^\mu(s)$ that lead to additional un-suppressed decoherence at the end of the QDD evolution.

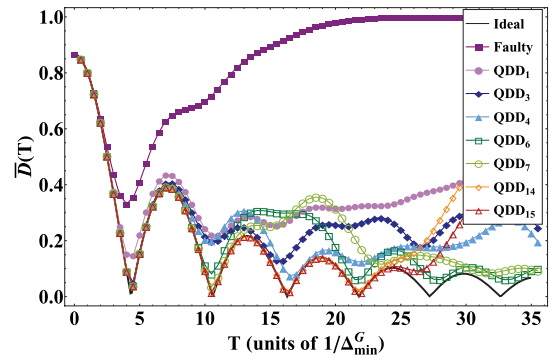


FIG. 12. (Color online) As in Fig. 11, for QDD with $M = \{1, 3, 4, 6, 7, 14, 15\}$. QDD-protected evolution deviates minimally from ideal evolution for $M = 15$ up to $T \approx 25/\Delta_{\min}^G$, thereafter $M = 6, 7$ are the optimal sequence orders. Unlike the CDD case, increasing the number of pulses does not result in closed-system-like behavior over the entire range of T considered. $M = 14, 15$ evolution closely coincides with ideal evolution more so than any other M values; however it also diverges faster than all order sequence orders at critical T values.

-
- [1] E. Farhi, J. Goldstone, S. Gutmann, and M. Sipser, [arXiv:quant-ph/0001106](https://arxiv.org/abs/quant-ph/0001106).
- [2] E. Farhi, J. Goldstone, S. Gutmann, J. Lapan, A. Lundgren, and D. Preda, *Science* **292**, 472 (2001).
- [3] D. Aharonov, W. van Dam, J. Kempe, Z. Landau, S. Lloyd, and O. Regev, *SIAM J. Comp.* **37**, 166 (2007).
- [4] J. Kempe, A. Kitaev, and O. Regev, *SIAM J. Comput.* **35**, 1070 (2006).
- [5] M. S. Siu, *Phys. Rev. A* **71**, 062314 (2005).
- [6] R. Oliveira and B. Terhal, *Quantum Inf. Comput.* **8**, 0900 (2005).
- [7] A. Mizel, D. A. Lidar, and M. Mitchell, *Phys. Rev. Lett.* **99**, 070502 (2007).
- [8] M. W. Johnson, M. H. S. Amin, S. Gildert, T. Lanting, F. Hamze, N. Dickson, R. Harris, A. J. Berkley, J. Johansson, P. Bunyk, E. M. Chapple, C. Enderud, J. P. Hilton, K. Karimi, E. Ladizinsky, N. Ladizinsky, T. Oh, I. Perminov, C. Rich, M. C. Thom, E. Tolkacheva, C. J. S. Truncik, S. Uchaikin, J. Wang, B. Wilson, and G. Rose, *Nature (London)* **473**, 194 (2011).
- [9] M. Steffen, W. van Dam, T. Hogg, G. Breyta, and I. Chuang, *Phys. Rev. Lett.* **90**, 067903 (2003).
- [10] X. Peng, Z. Liao, N. Xu, G. Qin, X. Zhou, D. Suter, and J. Du, *Phys. Rev. Lett.* **101**, 220405 (2008).
- [11] A. M. Childs, E. Farhi, and J. Preskill, *Phys. Rev. A* **65**, 012322 (2001).
- [12] M. S. Sarandy and D. A. Lidar, *Phys. Rev. Lett.* **95**, 250503 (2005).
- [13] J. Roland and N. J. Cerf, *Phys. Rev. A* **71**, 032330 (2005).
- [14] M. Tiersch and R. Schützhold, *Phys. Rev. A* **75**, 062313 (2007).
- [15] M. H. S. Amin, D. V. Averin, and J. A. Nesteroff, *Phys. Rev. A* **79**, 022107 (2009).
- [16] M. H. S. Amin, P. J. Love, and C. J. S. Truncik, *Phys. Rev. Lett.* **100**, 060503 (2008).
- [17] S. Jordan, E. Farhi, and P. W. Shor, *Phys. Rev. A* **74**, 052322 (2006).
- [18] D. A. Lidar, *Phys. Rev. Lett.* **100**, 160506 (2008).
- [19] A. M. Steane, *Phys. Rev. A* **68**, 042322 (2003).
- [20] E. Knill, *Nature (London)* **434**, 39 (2005).
- [21] B. M. Terhal and G. Burkard, *Phys. Rev. A* **71**, 012336 (2005).
- [22] D. Aharonov, A. Kitaev, and J. Preskill, *Phys. Rev. Lett.* **96**, 050504 (2006).
- [23] P. Aliferis, D. Gottesman, and J. Preskill, *Quant. Inf. Comput.* **6**, 97 (2006).
- [24] P. Aliferis and A. W. Cross, *Phys. Rev. Lett.* **98**, 220502 (2007).
- [25] In the circuit model a fault-tolerant simulation allows one to generate the output of a given ideal circuit, to arbitrary accuracy, using the faulty components of another circuit [71]. A similar definition for AQC would presumably involve the simulation of an ideal adiabatic evolution using a faulty one, but if “faulty” is simply taken to mean “nonadiabatic,” then one can just use the equivalence proof to argue that the problem is already solved. However, this argument misses the point since the defining feature of AQC—the adiabatic preparation of the ground state of H_p —should be preserved.
- [26] L. Viola and S. Lloyd, *Phys. Rev. A* **58**, 2733 (1998).
- [27] P. Zanardi, *Phys. Lett. A* **258**, 77 (1999).
- [28] L. Viola, E. Knill, and S. Lloyd, *Phys. Rev. Lett.* **82**, 2417 (1999).
- [29] E. Rains, *IEEE Trans. Inf. Theory* **45**, 266 (1999).
- [30] It can be shown [72] that in an appropriate rotating frame the DD protection technique of Ref. [18] is essentially equivalent to the method of energy-gap protection of AQC [17].
- [31] K. Khodjasteh and D. A. Lidar, *Phys. Rev. Lett.* **95**, 180501 (2005).
- [32] K. M. R. Audenaert and S. Scheel, *New J. Phys.* **10**, 023011 (2008).
- [33] R. Schützhold and G. Schaller, *Phys. Rev. A* **74**, 060304 (2006).
- [34] M. H. S. Amin and V. Choi, *Phys. Rev. A* **80**, 062326 (2009).
- [35] L. K. Grover, *Phys. Rev. Lett.* **79**, 325 (1997).
- [36] C. Bennett, E. Bernstein, G. Brassard, and U. Vazirani, *SIAM J. Comput.* **26**, 1510 (1997).

- [37] J. Roland and N. J. Cerf, *Phys. Rev. A* **65**, 042308 (2002).
- [38] A. T. Rezakhani, W.-J. Kuo, A. Hamma, D. A. Lidar, and P. Zanardi, *Phys. Rev. Lett.* **103**, 080502 (2009).
- [39] The linear interpolation in $H_{\text{ad}}^{2\text{SAT}}(t)$ is not optimal; see Ref. [73] for the optimal path. The 2-SAT on a ring problem is not associated with a quantum speedup (there exists a classical linear-time algorithm for 2-SAT [74]) but is instructive nonetheless and important in its own right as it corresponds to the preparation of the maximally entangled cat state $|\Phi_0^{2\text{SAT}}(T)\rangle$.
- [40] S. Sachdev, *Quantum Phase Transitions* (Cambridge University Press, Cambridge, 1999).
- [41] Given a set of clauses $\{C_j\}_{j=1}^n$ associated with n bits, such that each clause acts only on adjacent bits, the 2-SAT Hamiltonian acquires minimum energy when there are satisfying assignments for all clauses. In our transverse-field Ising model representation the clauses define agreement between adjacent bits (00 or 11, but not 01 or 10).
- [42] D. W. Ricker, *Echo Signal Processing* (Kluwer Academic Publishers, Boston, 2003).
- [43] In more detail, each random variable $\epsilon_j^\mu(t)$ can take values in $(-\infty, \infty)$ and they have a Gaussian noise correlation function [Fourier transform of the spectral density $S(\omega)$] $\langle \epsilon_j^\mu(t) \epsilon_j^\mu(t + \tau) \rangle = \frac{1}{\sqrt{2\pi}} \int_{-\infty}^{\infty} S(\omega) e^{-i\omega\tau} d\omega = \frac{J\beta}{\sqrt{2\pi}} \exp[-\frac{1}{2}(\tau\beta)^2]$; that is, a Gaussian with variance $1/\beta^2$ and amplitude $J\beta/\sqrt{2\pi}$, so that the amplitude of the fields $\epsilon_j^\mu(t) \propto \sqrt{J\beta}$. We note that since the spectral density $S(\omega) = \sqrt{\frac{J}{2\pi}} \exp[-\frac{1}{2}(\omega/\beta)^2]$ (i.e., the high-frequency cutoff is β), this means that as the noise amplitude grows, so does the cutoff, making the task for DD harder.
- [44] Here is why our noise model is equivalent to a random-unitary map. First, we simulate the dynamics of a quantum system subject to a randomly parametrized error Hamiltonian $H_{\text{err}}(t)$ given in Eq. (2). Let ϵ be the random variable parametrizing the error Hamiltonian, with distribution p_ϵ . Our simulations effectively generate random unitaries parametrized by ϵ (i.e., we generate an ensemble $\{p_\epsilon, U_\epsilon\}$). This yields a pure-state ensemble $\{p_\epsilon, |\psi_\epsilon\rangle\}$ where $|\psi_\epsilon\rangle = U_\epsilon|\psi_0\rangle$ and where $|\psi_0\rangle$ is the initial state. From the states that we compute for each new random realization of $H_{\text{err}}(t)$ we obtain the trace-norm distance $D_\epsilon := D[|\psi_\epsilon\rangle, |\psi_0\rangle] = \frac{1}{2} \|\psi_\epsilon - |\psi_0\rangle\|_1 = (1 - F_\epsilon^2)^{1/2}$, where $F_\epsilon = |\langle \psi_0 | \psi_\epsilon \rangle| = (1 - D_\epsilon^2)^{1/2}$ is the fidelity. Next we note that the following is a representation of a random-unitary map: $\rho = \sum_\epsilon p_\epsilon U_\epsilon |\psi_0\rangle\langle\psi_0| U_\epsilon^\dagger = \sum_\epsilon A_\epsilon |\psi_0\rangle\langle\psi_0| A_\epsilon^\dagger$, $A_\epsilon := \sqrt{p_\epsilon} U_\epsilon$. The fidelity squared for this channel is $F^2 = \langle \psi_0 | \rho | \psi_0 \rangle = \sum_\epsilon p_\epsilon \langle \psi_0 | U_\epsilon |\psi_0\rangle \langle \psi_0 | U_\epsilon^\dagger | \psi_0 \rangle = \sum_\epsilon p_\epsilon F_\epsilon^2 = 1 - \sum_\epsilon p_\epsilon D_\epsilon^2 = 1 - \bar{D}^2$. We define the average distance as $\bar{D} = \sum_\epsilon p_\epsilon D_\epsilon$ and this is the quantity shown in our plots. It is well known that in general the fidelity and trace-norm distance satisfy the inequality $1 - \bar{D} \leq F \leq (1 - \bar{D}^2)^{1/2}$, and so our plots give the lower bound $1 - \bar{D}$ on the fidelity of the random-unitary map.
- [45] Y. M. Galperin, B. L. Altshuler, J. Bergli, and D. V. Shantsev, *Phys. Rev. Lett.* **96**, 097009 (2006).
- [46] L. Cywiński, R. M. Lutchyn, C. P. Nave, and S. Das Sarma, *Phys. Rev. B* **77**, 174509 (2008).
- [47] From the AQC perspective, the $H_{\text{err}}(t)$ terms combine with $H_{\text{ad}}(t)$ to produce faulty operations by inducing random time-dependent fluctuations in the spectrum of $H_{\text{ad}}(t)$. In particular, these fluctuations also act to modify the size and location of the minimum energy gap Δ_{min} of H_{ad} .
- [48] The inclusion of pulse-width errors is left for a future study focusing on a more complete picture of fault tolerance; CDD is known to be relatively robust against such errors [31,49,50].
- [49] H. K. Ng, D. A. Lidar, and J. Preskill, *Phys. Rev. A* **84**, 012305 (2011).
- [50] G. A. Álvarez, A. Ajoy, X. Peng, and D. Suter, *Phys. Rev. A* **82**, 042306 (2010).
- [51] S. Blanes, F. Casas, J. Oteo, and J. Ros, *Phys. Rep.* **470**, 151 (2009).
- [52] L. Viola, E. Knill, and S. Lloyd, *Phys. Rev. Lett.* **85**, 3520 (2000).
- [53] K. Khodjasteh and D. A. Lidar, *Phys. Rev. A* **75**, 062310 (2007).
- [54] W. M. Witzel and S. Das Sarma, *Phys. Rev. B* **76**, 241303 (2007).
- [55] X. Peng, D. Suter, and D. A. Lidar, *J. Phys. B* **44**, 154003 (2011).
- [56] J. R. West, B. H. Fong, and D. A. Lidar, *Phys. Rev. Lett.* **104**, 130501 (2010).
- [57] G. S. Uhrig, *Phys. Rev. Lett.* **98**, 100504 (2007).
- [58] G. Quiroz and D. A. Lidar, *Phys. Rev. A* **84**, 042328 (2011).
- [59] W.-J. Kuo and D. A. Lidar, *Phys. Rev. A* **84**, 042329 (2011).
- [60] L. Jiang and A. Imambekov, *Phys. Rev. A* **84**, 060302 (2011).
- [61] The trace-norm distance $D[\rho_1, \rho_2] := \frac{1}{2} \|\rho_1 - \rho_2\|_1$, where $\|A\|_1 := \text{Tr}\sqrt{A^\dagger A}$, is a standard distance measure between quantum states [71]. When ρ_i is a pure state $\rho_i = |\psi_i\rangle\langle\psi_i|$ we replace the corresponding argument of D by $|\psi_i\rangle$.
- [62] S. Teufel, *Adiabatic Perturbation Theory in Quantum Dynamics* (Springer-Verlag, Berlin, 2003).
- [63] S. Jansen, M.-B. Ruskai, and R. Seiler, *J. Math. Phys.* **48**, 102111 (2007).
- [64] D. A. Lidar, A. T. Rezakhani, and A. Hamma, *J. Math. Phys.* **50**, 102106 (2009).
- [65] N. Wiebe and N. S. Babcock, *New J. Phys.* **14**, 013024 (2012).
- [66] Ideal-case oscillations are consistent with the adiabatic theorem, which predicts $D \rightarrow 0$ only in the limit $T \rightarrow \infty$. For an analytical expression predicting such oscillations in the case of Grover's algorithm see Ref. [75], Eq. (174).
- [67] This effect of open-system AQC, due to a competition between the benefit of increasing T for adiabaticity and the simultaneous increasing damage due to system-bath coupling, has been previously pointed out experimentally [9] and theoretically [12,76].
- [68] G. S. Uhrig, *New J. Phys.* **13**, 059504 (2011).
- [69] H. Uys, M. J. Biercuk, and J. J. Bollinger, *Phys. Rev. Lett.* **103**, 040501 (2009).
- [70] L. Cywiński, R. M. Lutchyn, C. P. Nave, and S. Das Sarma, *Phys. Rev. B* **77**, 174509 (2008).
- [71] M. A. Nielsen and I. L. Chuang, *Quantum Computation and Quantum Information* (Cambridge University Press, New York, 2000).
- [72] K. C. Young and M. Sarovar, (2012), [arXiv:1208.6371](https://arxiv.org/abs/1208.6371).
- [73] A. T. Rezakhani, D. F. Abasto, D. A. Lidar, and P. Zanardi, *Phys. Rev. A* **82**, 012321 (2010).
- [74] B. Aspvall, M. F. Plass, and R. E. Tarjan, *Inf. Process. Lett.* **8**, 121 (1979).
- [75] A. T. Rezakhani, A. K. Pimachev, and D. A. Lidar, *Phys. Rev. A* **82**, 052305 (2010).
- [76] M. S. Sarandy and D. Lidar, *Phys. Rev. A* **71**, 012331 (2005).